Food Hydrocolloids 106 (2020) 105926

Contents lists available at ScienceDirect

Food Hydrocolloids

journal homepage: http://www.elsevier.com/locate/foodhyd

Development of ovalbumin-pectin nanocomplexes for vitamin D_3 encapsulation: Enhanced storage stability and sustained release in simulated gastrointestinal digestion

Chuyue Xiang [a], Jian Gao [a], Haoxin Ye [a], Gerui Ren [a], Xiangjuan Ma [a], Hujun Xie [a,*], Sheng Fang [a,**], Qunfang Lei [b], Wenjun Fang [b]

[a] Lab of Food Colloid, School of Food Science and Biotechnology, Zhejiang Gongshang University, Hangzhou, 310018, People's Republic of China
[b] Department of Chemistry, Zhejiang University, Hangzhou, 310027, People's Republic of China

ARTICLE INFO

Keywords:
Ovalbumin
Pectin
Vitamin D_3
Encapsulation
Sustained release

ABSTRACT

Vitamin D_3 (VD_3) is a fat-soluble vitamin and easily degraded under acidic conditions, which will greatly reduce its bioavailability. The use of complexes formed by protein-polysaccharide to control release and protect active compounds has become a feasible way in the food field. In this work, ovalbumin (OVA) and high methoxyl pectin (PEC) were applied to fabricate OVA-PEC nanocomplexes to encapsulate and protect VD_3. The encapsulation efficiency of VD_3 by OVA-PEC complexes could reach to 96.37%, and the storage stability of VD_3 was obviously improved after encapsulation. The in vitro simulated gastrointestinal experiments combined with SEM and SDS-PAGE were employed to observe the digestive behavior of OVA-PEC-VD_3 nanocomplexes. A small amount of VD_3 is released from OVA-PEC-VD_3 nanocomplexes in simulated gastric fluid, while a large amount of VD_3 is released in simulated intestinal fluid. The sustained release kinetic of VD_3 from OVA-PEC-VD_3 nanocomplexes was consistent with the law of Higuchi model. The preliminary molecular mechanism for VD_3 encapsulation by OVA-PEC complexes was also investigated, and the formation of OVA-PEC-VD_3 nanocomplexes is ascribed to the electrostatic interactions, hydrogen bonding and hydrophobic interactions among OVA, PEC and VD_3. The results demonstrated that protein-polysaccharide complexes can effectively encapsulate VD_3 and achieve the goal of sustained release in the simulated gastrointestinal tract, which have potential applications in food and medicine.

1. Introduction

Vitamin D_3 (VD_3) is a nutrient substance and it is very important for human health. The lack of VD_3 will lead to osteoporosis, fragile bones, growth retardation and muscle weakness (Holick, 2007). VD_3 is also a fat-soluble ingredient, unstable to light, and easily oxidatively decomposed in air. These limitations in its own nature greatly reduce its bioavailability (Levinson, Ish-Shalom, & Segal, 2016), thus it is necessary to develop a suitable delivery system to add VD_3 into foods to increase the intake of VD_3.

The raw materials used in the preparation of delivery systems for the food industry must be food-grade, and biopolymer nanoparticles prepared using protein and polysaccharide are considered to be one of the most promising pathways for the preparation of food-grade delivery systems (Burey, Bhandari, & Howes, 2008; Chen et al., 2020; Chen, Subirade, & Remondetto, 2006; Jones & McClements, 2010; Rostami, Yousefi, & Khezerloua, 2019; Xie et al., 2019). Protein and polysaccharide are two important macromolecules in foods that affect the nutritional properties (Huang et al., 2020; Schmidt, Novales, & Boué, 2010) and the texture of foods. The whey protein isolate (WPI) was employed to prepare nanoparticle for VD_3 encapsulation (Abbasi, Emam-Djomeh, & Mousavi, 2014), which effectively increased the storage stability of vitamins. The α-lactoglobulin (Delavari et al., 2015) and β-lactoglobulin (Diarrassouba et al., 2013) were used to encapsulate VD_3, respectively, and found that proteins can bind to VD_3 through hydrophobic interactions, thereby increasing VD_3 stability and bioavailability. Recently, the vitamin D_3-fortified nanoemulsions were fabricated acting as a carrier to improve the vitamin bioaccessibility (Schoener, Zhang, & Lv, 2019). The casein micelles were also applied to encapsulate VD_3 (Cohen et al., 2017), and demonstrated that the in vitro

* Corresponding author.
** Corresponding author.
E-mail addresses: hujunxie@gmail.com (H. Xie), fszjgsu@163.com (S. Fang).

https://doi.org/10.1016/j.foodhyd.2020.105926
Received 27 December 2019; Received in revised form 6 March 2020; Accepted 7 April 2020
Available online 12 April 2020

bioavailability of VD_3 in Caco-2 cell models is improved after encapsulation. However, there are still few studies on how to increase the encapsulation efficiency of VD_3 and enhance its sustained release in simulated gastrointestinal tract. Therefore, it is essential to develop a delivery system to increase the water solubility, stability, and encapsulation efficiency for VD_3, and achieves the purpose of sustained release in simulated gastrointestinal tract.

Egg white is rich in nutrients and has excellent functional properties (foaming, emulsifying, gelling, etc.). The main protein in egg white is ovalbumin (OVA) with a molecular weight of about 45 kDa (Li et al., 2018). OVA is a typical globulin consisting of 385 amino acids, and adopts a serpin-like structure (Li et al., 2014; Maste, Norde, & Visser, 1997). OVA is also an important food ingredient and has been widely used in the food industry due to its emulsifying and stabilizing properties and foam stability (Niu et al., 2015). Surprisingly, OVA exhibits the characteristics of anti-mutation and anti-cancer (Vis, Plinck, & Alink, 1998), immunomodulatory and antioxidant properties (Souza & Garcia-Rojas, 2015). Based on which, OVA has been widely used as a model protein in the study of protein structure and functional properties (Lii, Chen, & Lu, 2003). Feng et al. (2019) used OVA and sodium alginate to prepare nanocomplexes for curcumin (Cur) vehiculization, and the results showed that it can effectively improve the bioavailability and stability of Cur.

Pectin (PEC) is a soluble dietary polysaccharide existed in almost terrestrial plants with a pKa value of about 3.6. It has good gel properties and can be used to make jelly and jam, and stabilize acidic protein beverages (Humblet-Hua, Scheltens, & van der Linden, 2011; Ru, Wang, & Lee, 2012). According to the degree of methoxylation (DM), pectin can be divided into two categories including low methoxyl pectin and high methoxyl pectin. In general, high methoxyl pectin (DM > 50%) with low concentration and pH allow the formation of a gel, while the formation of a gel with low methoxyl pectin (DM < 50%) requires to add a divalent metal ion to form an egg box structure (Ström, Schuster, & Goh, 2014).

Over the past few years, the complexes formed by protein and polysaccharide are used to protect and control release functional factors and have become one of the research hotspots in the food field. Protein-polysaccharide complexes tend to have better functional properties than proteins or polysaccharides alone (Schmitt, Sanchez, & Desobry-Banon, 1998). In this manuscript, OVA and PEC (DM > 50%) were used as building blocks to prepare OVA-PEC nanocomplexes for VD_3 encapsulation in order to increase its water solubility and achieve sustained release. The preliminary molecular mechanism of VD_3 encapsulation by OVA-PEC complexes was investigated. Furthermore, the release kinetics of VD_3 from OVA-PEC-VD_3 nanocomplexes under simulated gastric and intestinal fluids were determined and discussed.

2. Materials and methods

2.1. Materials

Ovalbumin (OVA, purity > 98%), pectin (PEC, galacturonic acid > 74%, M_w = 736889), vitamin D_3 (VD_3, purity > 98%), pepsin (activity: 3000 U/mg), pancreatin (USP, Aladdin P110505), NaOH, HCl, NaCl, Sodium dodecyl sulfate (SDS), Na_2HPO_4, sodium cholate, anhydrous citric acid and sodium deoxycholate monohydrate were bought from Aladdin Chemical Co., Ltd. All other chemicals are analytical grade, and deionized water was selected for experiments.

2.2. Methods

2.2.1. OVA-PEC-VD_3 nanocomplexes preparation

A certain amount of OVA and PEC were dissolved in buffer (pH = 7) to reach the final concentration of 0.05 wt%. The solution was stirred at 400 rpm for 2 h at room temperature, and then stored in a 4 °C refrigerator overnight. VD_3 was dissolved in ethanol. The antisolvent precipitation (ASP) method was used to prepare the complexes. VD_3 was dissolved in ethanol. The VD_3 ethanol solution was injected into the OVA solution under stirring. Then the ethanol in this system was removed by rotary evaporation. The obtained OVA-VD_3 solution was added to the PEC solution (mass ratio OVA:PEC = 2:1). The mass ratio of OVA and PEC was optimized by turbidity measurement. The pH of the system was adjusted to the desired value using NaOH and HCl solutions to obtain a complex solution.

2.2.2. The preparation of OVA-PEC-VD_3 complex coacervate

The concentration of OVA-PEC-VD_3 complex solution was expanded to 1 wt%, and the lower phase was collected by freeze centrifugation, followed by freeze drying for 48 h to obtain the complex coacervate.

2.2.3. Gel permeation chromatography (GPC)

Waters 515 Gel permeation chromatography was used to measure the molecular weight of PEC. PEC (50 mg) was accurately weighed and dissolved in 10 ml NaCl solution (0.1 mol/L), and the sample was obtained by filtration with a 0.45 μm membrane.

2.2.4. Turbidity measurement

The absorbance of the sample at 25 °C was measured using an ultraviolet spectrophotometer (UV-2600, Shimadzu, Japan) at a wavelength of 400 nm. The turbidity was defined as 1-T (transmittance, cm^{-1}) (Souza & Garcia-Rojas, 2015), and each sample was measured three times.

2.2.5. ζ-Potential and particle size measurement

The ζ-potential value, particle diameter, and polydispersity index (PDI) were measured through a Nano-ZS type laser particle size analyzer (Malvern, UK). All tests were performed at a refractive index of 1.450 and 25 °C (Fang, Zhao, & Liu, 2019). Each test scans for twelve times and each sample was taken for three times.

2.2.6. VD_3 loading

A series of gradient concentrations of VD_3 ethanol solutions were prepared. The absorbance of these solutions were measured at a wavelength of 265 nm to obtain a standard curve with R^2 of 0.9997 as shown in Fig. S1 (see Supporting Information). The effect of different pH values (2.6, 2.7, 2.8, 2.9, 3.0, 3.2, 3.4) and different VD_3 concentrations (2.5, 5, 7.5, 10, 12.5, 15 mg/L) on the encapsulation efficiency (*EE*) were investigated. The encapsulation efficiency (*EE*) and loading capacity (*LC*) were calculated according to equations (1) and (2), respectively.

$$EE(\%) = \frac{\mathrm{TotalVD3} - \mathrm{FreeVD3}}{\mathrm{TotalVD3}} \times 100\% \quad (1)$$

$$LC(\%) = \frac{\mathrm{TotalVD3} - \mathrm{FreeVD3}}{\mathrm{WeightofOVA} - \mathrm{PECcomplex}} \times 100\% \quad (2)$$

2.2.7. Morphology

The complex solution (0.05 wt%) was dropped on a copper grid, counter-dyed with uranyl acetate. Then the microstructure of the complex was obtained by transmission electron microscope (TEM, JEM-1200EX, Japan) with a working voltage of 200 kV.

2.2.8. Storage stability

The OVA-PEC-VD_3 nanocomplexes was stored at 4 °C for 31 d, and a portion of solutions was taken every 10 d to measure the particle size and PDI changes during storage.

2.2.9. In vitro release study

An in vitro simulated digestion model was established based on previous methods (Feng et al., 2019; Qiu et al., 2018) with slight modification to study the sustained release of VD_3. The simulated gastric fluid (SGF) was prepared accordingly. 0.4 g of NaCl solid powder and

0.64 g of pepsin were dissolved in a small amount of deionized water. The solution was added with 1.4 mL HCl, then volumed to 200 mL with deionized water. After fully dissolved, the solution was preheated in a constant temperature water bath at 37 °C. The simulated intestinal fluid (SIF) was prepared as follows. 30.72 mM NaCl, 0.30 mM $CaCl_2$, 5 mg/mL bile salt (sodium cholate and sodium deoxycholate mixed with a mass ratio of 1:1) and 8 mg/mL pancreatin were added to 200 mL deionized water. After fully dissolved, the supernatant was taken by high-speed refrigerated centrifugation and put in a 37 °C water bath to preheat.

The OVA-PEC-VD_3 nanocomplexes were preheated in a 37 °C water bath for 10 min, and then added into the SGF in a volume ratio of 1:1, and the pH of this mixture was quickly adjusted to 2. The mixed solution was put in a shaker at 37 °C and 100 rpm. After 60 min, the chyme from the gastric phase was mixed with the preheated SIF in a 1:1 vol ratio, and the pH of the system was quickly adjusted to 7, and placed in a 37 °C shaker for simulated digestion at 270 rpm. Samples were collected at preset time intervals, then loaded into ultrafiltration centrifuge tubes with a cut-off molecular weight of 3k and centrifuged at 4500 rpm for 20 min to obtain free VD_3. Free VD_3 concentration was determined according to the standard curve as shown in Fig. S1 (see Supporting Information). The complex system was replaced with a buffer, mixed with the SGF and SIF under the same conditions as a blank control. The absorbance of blank control was subtracted from the actual calculation.

The cumulative release rate of VD_3 was calculated by equation (3).

$$\text{Cumulative release rate } (\%) = \frac{C \times V}{M} \times 100\% \quad (3)$$

where C represents the VD_3 concentration released from the mixed solution (mg/L), V represents the volume (mL) of the solution, and M represents the amount of VD_3 including in nanocomplexes (mg).

The proteolysis of OVA-PEC-VD_3 nanocomplexes was investigated via sodium dodecyl sulfate-polyacrylamide gel electrophoresis (SDS-PAGE) analysis, which was carried out with 15% separation gel and 5% stacked gel. Took an aliquot (12 μL) from the digestion fluid at different digestion time and instantly mixed with 4 μL of loading buffer, containing 313 mmol/L Tris-HCl (pH = 6.8), 0.05% bromophenol blue, 50% glycerol, 10% SDS, and boiled for 5 min. The electrophoresis was performed in electrophoresis cells (Minipretein III, Bio-Rad, USA) and electrophoresed at 80 V for 20 min, and then electrophoresed at 160 V for 50 min. The gel was stained with Coomassie Blue R-250 for 60 min and decolorized with a solution containing 10% methanol and 7.5% acetic acid. The samples were decolorized 3 times for 30 min each. Gel images were taken using Alpha View SA Imager (Protein simple, USA).

2.2.10. Morphological changes of nanocomplexes during simulated digestion

The morphology of samples after 0, 30, 60, 90, 120, and 180 min of simulated digestion was investigated by scanning electron microscopy (SEM, SU8010, Hitachi, Japan).

2.2.11. Fluorescence spectroscopy

The fluorescence spectra were measured using fluorescence spectrophotometer (F-7000, Hitachi, Japan). The concentrations of OVA and OVA-PEC complexes were both 0.5 mg/mL, the OVA:PEC mass ratio was 2:1, and the VD_3 concentrations were 0, 2.5, 5, 7.5, 10, 12.5, 15 mg/L, respectively. The excitation light wavelength was 290 nm. The excitation and emission slit width were both 5 nm, and the scanning range was 300–450 nm. The range of synchronous scanning was $\lambda_{ex} = 220$ nm, $\lambda_{em\,(a)} = 235$ nm, and $\lambda_{em(b)} = 280$ nm, where the difference of wavelengths ($\Delta\lambda$) were 15 nm and 60 nm, respectively.

2.2.12. FTIR spectra

Controlled the mass ratio of sample:KBr = 1:100, and the ground mixed powder was pressed into a uniform transparent sheet by a tableting machine. The sample was scanned 16 times in the wavelength range of 4000-400 cm^{-1} using a Fourier transform spectrophotometer (Nicolet iS5, Thermo Fisher, USA) at room temperature (three times in parallel).

2.2.13. Statistical analysis

Each experiment was repeated three times. The experimental data were in the form of mean ± standard deviation. One-way ANOVA was carried out on the data using SPSS 18.0 software, and the significance level was 5%.

3. Results and discussion

3.1. Optimization condition for the preparation of complexes

From the turbidity experiments of different OVA/PEC mass ratios (Fig. 1a), it can be seen that when the mass ratio of OVA and PEC is 2:1, the adsorption of OVA on PEC is saturated, which has a certain influence on the formation of nanocomplexes. Therefore, OVA:PEC = 2:1 was used as one of the conditions for the preparation of the OVA-PEC-VD_3 nanocomplexes. Other preparation conditions were optimized by comparing the particle size, ζ-potential and encapsulation efficiency (*EE*) at different pH values.

As shown in Fig. 1c, the OVA-PEC-VD_3 nanocomplexes have a small particle size of about 250 nm and small PDI at pH = 2.8, and the particle size distribution in the system is relatively uniform. Moreover, it has relatively strong electrostatic interactions between OVA and PEC (Fig. 1b). Fig. 1d shows the *EE* of OVA-PEC complexes for VD_3 and the ζ-potential of OVA-PEC-VD_3 nanocomplexes at different pH values. The absolute value of ζ-potential of complexes decreases with the decrease of pH, and the charge on the surface of complexes is close to zero. Thus the electrostatic repulsions between complex particles are reduced, and aggregation tends to occur and leads to the increase of average particle size. With the increase of pH value, the encapsulation efficiency of VD_3 by OVA-PEC complexes increases firstly and then decreases. The optimized conditions for the preparation of OVA-PEC-VD_3 nanocomplexes was as follows. The mass ratio of OVA and PEC is 2:1 and pH is equal to 2.8.

3.2. Encapsulation efficiency and loading capacity

Fig. 2 describes the *EE* and *LC* of OVA-PEC complexes for the encapsulation of VD_3. As the concentration of VD_3 increases, *EE* is firstly increased and then decreased. When the concentration of VD_3 reaches to 10 mg/L, the OVA-PEC complexes have the highest *EE* of about 96.37%, and the *LC* is 1.93%. VD_3 is difficult to dissolve in the buffer, while VD_3 encapsulated by the OVA-PEC complexes is well dispersed in the buffer, indicating that the interactions among OVA, PEC and VD_3 promote the dissolution of VD_3 in the buffer. The results showed that the OVA-PEC complexes have a good encapsulation effect for VD_3.

3.3. TEM observation

The microstructure of OVA and VD_3-loaded OVA-PEC nanocomplexes were observed by TEM as shown in Fig. 3. It can be seen that the size of OVA particles is small, and large aggregate can be found due to the dehydration treatment before observation. The self-assembly of OVA molecule does not occur to form large nanoparticles at pH = 7, while the morphology of VD_3-loaded OVA-PEC nanocomplexes appears as spherical nanoparticles with regular shapes. In combination with the DLS experiments, the average particle size of OVA is about 9.7 ± 1.34 nm, while the average particle size of OVA-PEC-VD_3 nanocomplexes is about 249.75 ± 5.45 nm, which was larger than that of OVA alone. This may be attributed to the interactions among PEC, VD_3 and OVA.

The particle size observed by TEM is slightly smaller than that of DLS. This is due to that the sample was hydrated during DLS

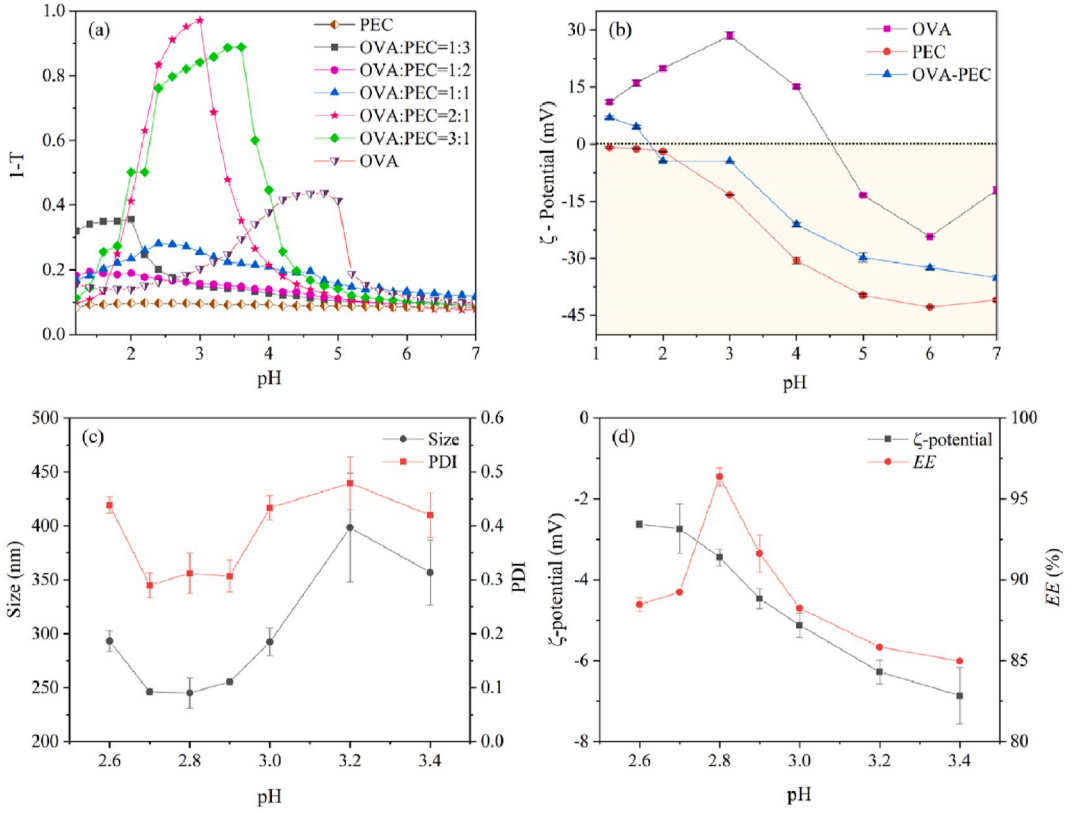

Fig. 1. Optimization of preparation conditions for OVA-PEC-VD_3 nanocomplexes at different pH. (a) Turbidity (1-T) curves of OVA, PEC, OVA-PEC complex solutions at different mass ratios (0.05 wt%). (b) ζ-Potential of OVA (0.025 wt%), PEC (0.025 wt%) and OVA-PEC (2:1, 0.05 wt%) complex solutions at different pH. (c) Size and PDI. (d) ζ-Potential and *EE* for VD_3 (OVA:PEC = 2:1, the concentration of VD_3 = 10 mg/L).

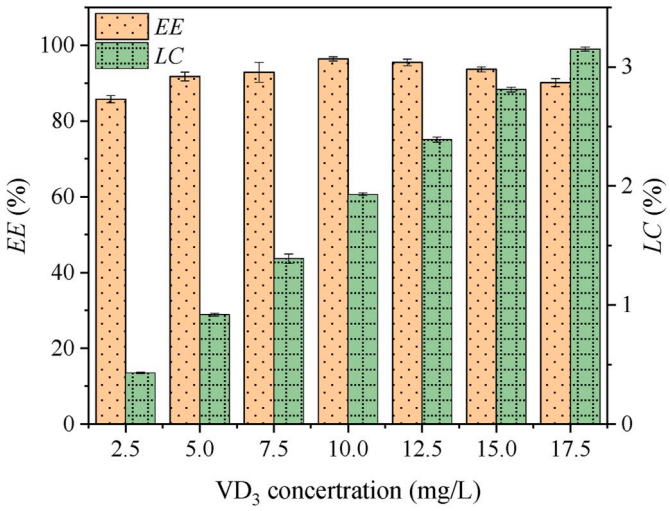

Fig. 2. The encapsulation efficiency (*EE*) and loading capacity (*LC*) for VD_3 by OVA-PEC complexes.

measurement, while it was dehydrated during TEM observation (Lin et al., 2015).

3.4. Storage stability

The shelf life of foods is very important in commercial applications, so the OVA-PEC-VD_3 nanocomplexes should be stable throughout the shelf life. By measuring the change of particle size and polydispersity index (PDI) during storage, it can determine whether the complex has good storage stability. As shown in Fig. 4, the PDI of complexes is between 0.08 and 0.7 and only slightly fluctuates over time, indicating that the distribution of particle size is relatively uniform during storage.

During the 31-day storage period, the particle size of OVA-PEC-VD_3 nanocomplexes increases by 58 nm from 249.75 nm to 307.71 nm. No turbidity or obvious floc appears in the samples, indicating that the OVA-PEC-VD_3 nanocomplexes exhibits high stability to meet the stability requirement for commercial use.

3.5. Sustained-release behavior of nanocomplexes by in vitro simulated digestion

3.5.1. In vitro release study

The environment of the human gastrointestinal tract is complicated due to the large difference in pH, and a large number of digestive enzymes such as pepsin and pancreatin, as well as salt ions, thus the food function factors are extremely easily digested and metabolized, and it is difficult to achieve the purpose of targeted release. In this work, the digestive behavior of OVA-PEC-VD_3 nanocomplexes in SGF and SIF were studied in order to achieve sustained release.

Initially, the OVA-PEC-VD_3 nanocomplexes were digested in SGF for 60 min, and then rapidly added into SIF for 120 min. The cumulative release rate of VD_3 was determined at a different time as described in Fig. 5a. It can be seen that the release rate of VD_3 in SGF from OVA-PEC-VD_3 nanocomplexes is very low. The release rate of VD_3 only reaches to 11.25% after 60 min of simulated gastric digestion. Once digestion begins in SIF, the cumulative release rate increases sharply within 30 min, and then becomes flat and reaches the cumulative release rate of 98.39%.

Protein hydrolysis is closely involved in the release and degradation of encapsulated VD_3, as it is the basis for the delivery system. The OVA proteolysis in simulated digestion was studied by SDS-PAGE (Fig. 5b).

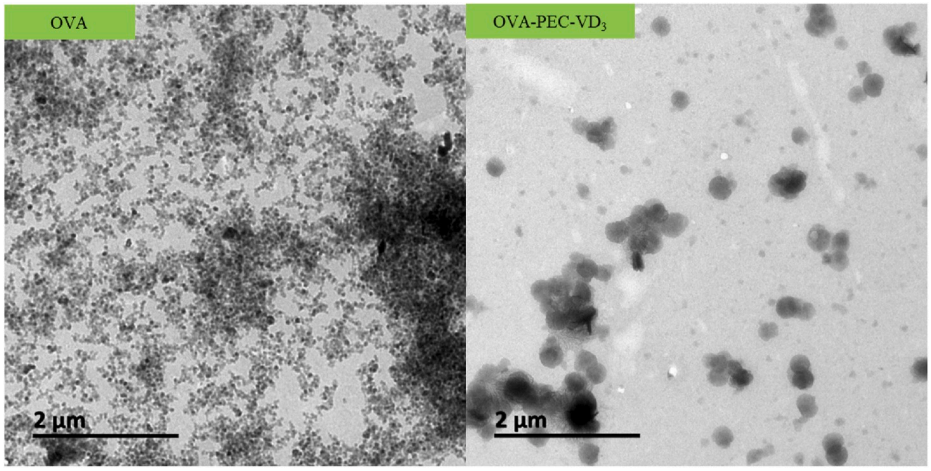

Fig. 3. TEM images of OVA and OVA-PEC-VD_3 nanocomplexes.

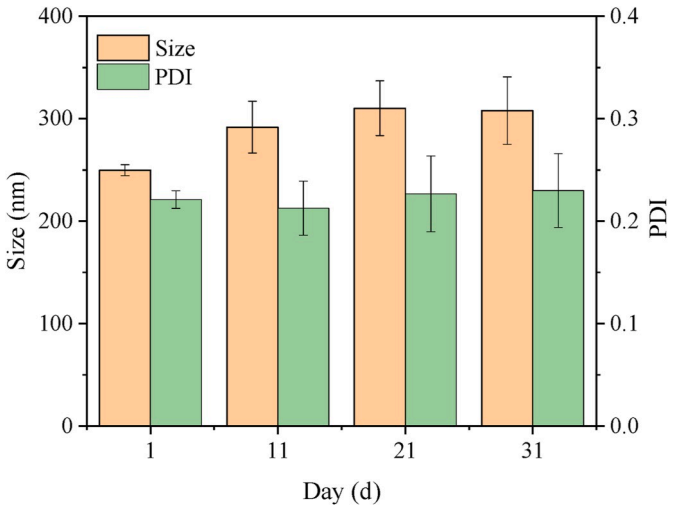

Fig. 4. Effect of different storage time on the stability of OVA-PEC-VD_3 nanocomplexes.

The complex sample shows a dense OVA band at 45–60 kDa before digestion (0 min), and most of the OVA bands are still retained in SGF, indicating that OVA-PEC-VD_3 nanocomplexes are resistant to pepsin. The interfacial PEC chain protects the cleavage site of pepsin on OVA, thereby inhibiting the rate and extent of proteolysis. Pepsin and PEC chains are negatively charged under SGF conditions, and the electrostatic repulsions lead to limited pepsin binding to OVA-PEC-VD_3 nanocomplexes (Feng et al., 2019; Sarkar, Zhang, & Murray, 2017).

However, the nanocomplexes are easily hydrolyzed in SIF. The intact OVA band disappears rapidly, and VD_3 is almost completely released from the nanocomplexes after the SIF digestion. The structure of OVA-PEC-VD_3 nanocomplexes will dissociate or swell under neutral conditions, thereby promoting intestinal fluid penetration. In addition, adsorbed polysaccharide chains can be replaced by the bile salts with high surface-active and disrupt the conformation of the protein, thereby accelerating its proteolysis (Martos, Contreras, & Molina, 2010).

Fig. 5c shows the SEM image of morphological changes of OVA-PEC-VD_3 nanocomplexes during simulated digestion. The OVA-PEC-VD_3 nanocomplexes have distinct grain structure in SGF, and the particle size increases along with time, which indicates that the nanocomplexes have slight swelling behavior in SGF.

When the complexes enter into SIF, no particle structure can be observed in the system. The interactions between OVA and PEC are weakened in SIF, and the protein is exposed to SIF cleaved by the enzyme. Finally, the structure of OVA-PEC-VD_3 nanocomplexes is destroyed to become chyme, and VD_3 is released in large quantities.

3.5.2. *Modeling release kinetics in SGF and SIF*

In order to further investigate the release mechanism of VD_3 from OVA-PEC-VD_3 nanocomplexes in simulated digestion experiments, the nanocomplexes were placed in SGF and SIF for 180 min, respectively, and the cumulative release rate of VD_3 was determined to establish release kinetic model. The Higuchi, first-order kinetic and zero-order kinetic models were used to fit the release rate of nanocomplexes in the simulated digestion experiments (Table 1). The zero-order kinetics model defines the release of active ingredients at a constant rate. The first-order kinetics model is common for matrix-type encapsulation, explaining the drug release profile of water-soluble drugs in a porous matrix (Akyuz, 2020; Kaya, Kucukada, & Alemdar, 2019). Higuchi model is based on Fickian diffusion, and it was improved by Higuchi in order to explain the release of active ingredient from solid matrix (Higuchi, 1963).

Three models are reasonable and the Higuchi model shows the highest fitting coefficients, indicating that the release of VD_3 from OVA-PEC-VD_3 nanocomplexes is consistent with the law of Higuchi model, and the overall release is closer to Fick release. According to the Higuchi model, there is a linear relationship between the cumulative release rate of VD_3 and the square root of the simulated digestion time (Fig. 6a and b).

Pepsin is a proteolytic enzyme that tends to cleave peptide bonds of hydrophobic amino acids in proteins when it cleaves proteins, destroying the structure of proteins. After protein and polysaccharide form complexes, the hydrophobic amino acid of protein tends to be protected in the inner core region, thereby forming a protective outer shell and reducing the damage of pepsin, thus it remains relatively stable. VD_3 can bind to the hydrophobic core of the protein, and strong interactions between protein and polysaccharide still existed in simulated gastric fluid. The shell formed by protein and polysaccharide prevents the digestion of VD_3 by pepsin, thus only a small amount of VD_3 is released in SGF. When the complex enters into SIF, the interactions between protein and polysaccharide are significantly weakened due to the change of environmental pH. The protein is exposed to SIF, and the pancreatin destroys the conformation of the protein, resulting in the large release of VD_3. It can be seen that the encapsulated VD_3 has a good sustained-release effect.

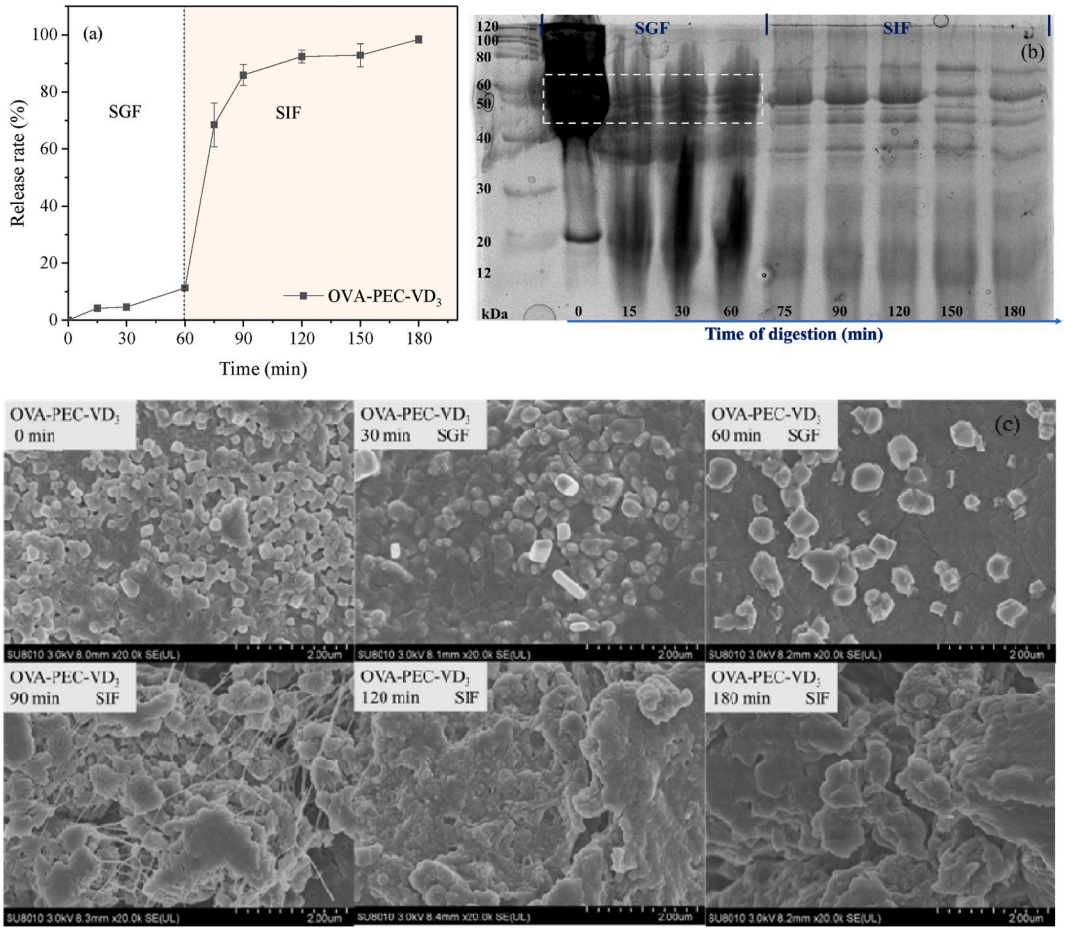

Fig. 5. In vitro simulated digestion experiments. (a) The release rate of VD_3 from OVA-PEC-VD_3 nanocomplexes. (b) SDS-PAGE patterns. (c) SEM images of OVA-PEC-VD_3 nanocomplexes at different digestion time.

Table 1
Kinetic model fitting results.

Kinetic model	Release mechanism	Equation	R^2	
			SGF	SIF
Zero-order	Constant speed release	$Q = Q_0+kt$	0.846	0.854
First-order	First release	$Ln(1-Q) = -kt$	0.808	0.913
Higuchi	Fick release	$Q = kt^{1/2}$	0.981	0.985

Where Q is the cumulative release rate of VD_3 in the simulated digestion time t, and Q_0 is the initial amount of VD_3 in OVA-PEC-VD_3 nanocomplexes (usually, $Q_0 = 0$), and k is the release constant.

3.6. Molecular mechanism for VD_3 encapsulation by OVA-PEC complexes

3.6.1. Fluorescence quenching mechanism of VD_3 with OVA and OVA-PEC complexes

Fluorescence spectroscopy can be used to study the conformation of proteins in aqueous solutions. When proteins react with drug molecules, they can cause changes in the fluorescence properties of the system. Three main mechanisms for fluorescence quenching are possible including non-radiative energy transfer, static quenching and dynamic quenching, and the latter two agree with the Stern-Volmer equation.

$$F0 / F = 1 + Kq\tau 0Q = 1 + KSVQ \quad (4)$$

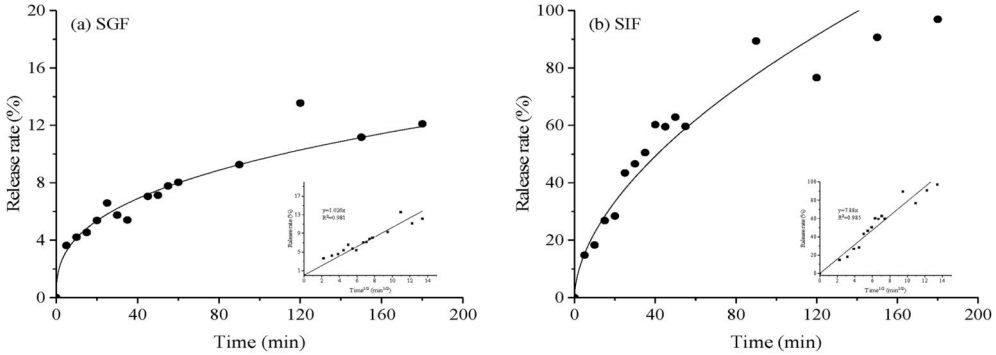

Fig. 6. Fitting of release kinetics equation ($Q = kt^{1/2}$) to VD_3 released from OVA-PEC-VD_3 nanocomplexes in simulated gastric fluid (SGF) (a) and simulated intestinal fluid (SIF) (b).

where F describes the fluorescence intensity when there is a quencher, F_0 describes the fluorescence intensity when there is no quencher, Q describes the concentration of quencher, K_{SV} describes the quenching constant, K_q describes the quenching rate constant, and τ_0 describes average lifetime of molecule in the absence of quencher (10^{-8} s) (Papadopoulou, Green, & Frazier, 2005; Yu et al., 2011).

Dynamic fluorescence quenching can be occurred by a collision between fluorophore and quencher, which is caused by a complex that forms a ground state between fluorophore and quencher. The increase of temperature leads the decrease of fluorescence intensity, and for static quenching, the corresponding K_{SV} of elevated temperature also decreases. To further investigate the quenching mechanism of VD_3 for OVA and OVA-PEC complexes, fluorescence measurements were performed at 25 °C and 35 °C. It can be seen from Fig. 7a and b that the fluorescence intensity of OVA emission peak decreases regularly with the increasing VD_3 concentration, indicating that the interactions between OVA and VD_3 cause the endogenous fluorescence of protein to be quenched regularly. In addition, the fluorescence intensity decreases with the increase of temperature. The quenching rate constant of VD_3 to OVA is larger than the maximum diffusion collision quenching rate constant of 2×10^{10} L·mol^{-1}·s^{-1}, so the quenching of OVA via VD_3 is mainly static quenching. By comparing the quenching constants at different temperatures, $K_{SV} = 2.13 \times 10^4$ L·mol^{-1} (25 °C) and $K_{SV} = 2.38 \times 10^4$ L·mol^{-1} (35 °C), the quenching constant is increased with the increase of temperature, indicating that dynamic quenching in the system is not negligible. Similar results have also been found in previous work (Yu et al., 2011).

Fig. 7c and d show the fluorescence quenching spectra of OVA in OVA-PEC complex by VD_3. With the increase of VD_3 concentration, the fluorescence intensity decreases regularly, and the fluorescence intensity of OVA-PEC-VD_3 complex is lower than that of OVA alone. By calculating and comparing the quenching constant $K_{SV} = 1.69 \times 10^4$ L·mol^{-1} (25 °C) and $K_{SV} = 1.82 \times 10^4$ L·mol^{-1} (35 °C) at different temperatures, it is known that the quenching constant increases with the increase of temperature, and the quenching rate constant (K_q) of VD_3 for OVA-PEC is much larger than 2×10^{10} L·mol^{-1}·s^{-1}, indicating that the main quenching mechanism of VD_3 to OVA-PEC is static quenching, while dynamic quenching also exists.

The binding constant (K_a) and binding site (n) of VD_3 to OVA and OVA-PEC complexes can also be calculated via analyzing the fluorescence intensity data. The relationship is as follows (Yang, Wu, & Li, 2013).

$$\log \frac{(F0 - F)}{F} = \log Ka + n \log[Q] \quad (5)$$

where F and F_0 describe the fluorescence intensity of OVA with and without VD_3, Q describes the concentration of VD_3 added, K_a describes the binding constant, and n describes the number of binding sites on each OVA.

According to the inset of Fig. 7, K_a and n are calculated, and the specific data are described in Table 2. The binding constant K_a of VD_3 to OVA and OVA-PEC complex are between 10^4-10^6 L·mol^{-1}, which indicates that the complexes are relatively stable, and the OVA-PEC complexes can be used as a carrier for VD_3. As the temperature increases, the binding constants of VD_3 to the OVA and OVA-PEC

Table 2
Binding constants and binding sites of VD_3 with OVA and OVA-PEC complexes.

Samples	T (K)	K_a (L·mol^{-1})	n	R^2
OVA	298	2.13×10^4	1.168	0.975
	308	2.38×10^4	1.281	0.994
OVA-PEC	298	1.69×10^4	0.611	0.903
	308	1.82×10^4	0.727	0.872

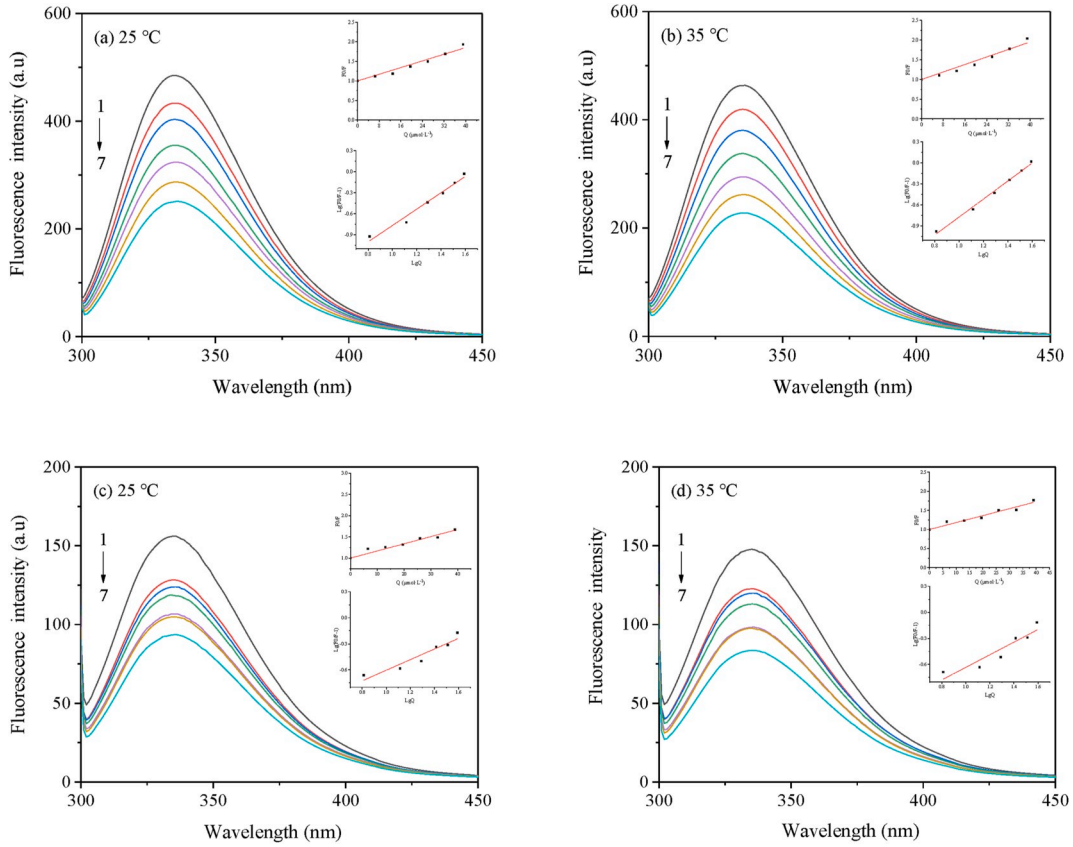

Fig. 7. Fluorescence emission spectra of OVA-VD_3 at 25 °C (a) and 35 °C (b), OVA-PEC-VD_3 at 25 °C (c) and 35 °C (d).

complexes increase, indicating that VD_3 is combined with the OVA and OVA-PEC complexes through hydrophobic interaction, and VD_3 is embedded in the hydrophobic group of OVA.

3.6.2. Synchronous fluorescence spectroscopy

Synchronous fluorescence spectroscopy can provide insights into the effect of VD_3 on protein conformation, and synchronous fluorescence spectra at $\Delta\lambda = 15$ nm and $\Delta\lambda = 60$ nm reflect the changes of micro-environment around tyrosine and tryptophan residues, respectively (Liu, Wu, & Yang, 2010). If the maximum emission wavelength of the fluorescence of residues is red-shifted, it means that the polarity of the amino acid residue is enhanced, whereas the blue shift means that the hydrophobicity of the amino acid residue is enhanced (Hu et al., 2006). The synchronous fluorescence spectra of OVA and OVA-PEC complexes after adding different VD_3 concentrations are displayed in Fig. 8. When the concentration of VD_3 is increased, the fluorescence intensity is decreased. A slight red shift in the fluorescence spectra indicates that the secondary structure of OVA has changed due to the binding between VD_3 and PEC, and the polarity of amino acid residue has also been enhanced.

3.6.3. The interaction between VD_3 and OVA-PEC complex by FTIR

FTIR analysis was performed to determine the possible mechanism for the formation of nanocomplexes among VD_3, OVA and PEC (Fig. 9). The band of 3100–3500 cm^{-1} is caused by the vibration of O–H bond of a hydroxyl group (Liang et al., 2015). The characteristic peaks of PEC are the broad peaks caused by stretching vibration of O–H bond at 3145 cm^{-1}, and the peak at 1748 cm^{-1} is caused by stretching of esterified carbonyl and 1643 cm^{-1} is caused by stretching of carboxylate anion (Chang et al., 2017), and the carboxylate anion also exhibits multiple weak vibrations between 950 cm^{-1} and 1300 cm^{-1} (Hu, Wang,

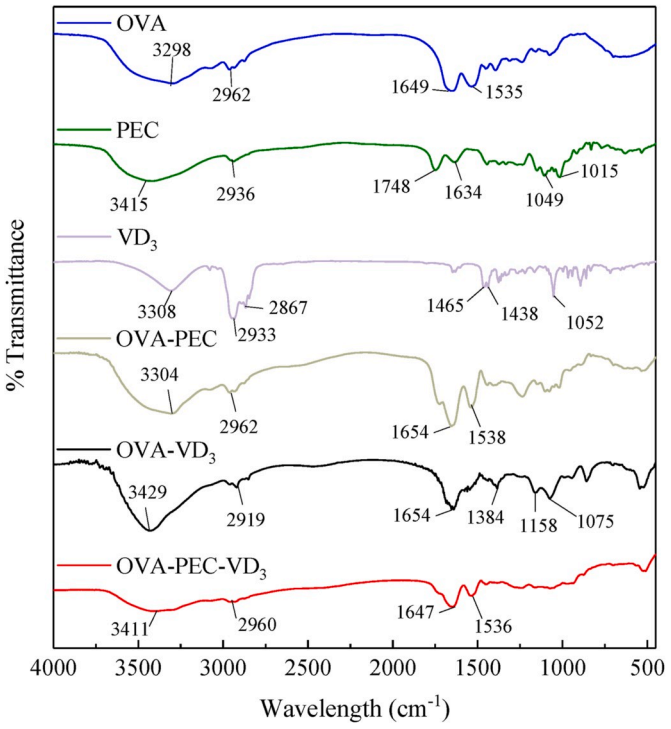

Fig. 9. FTIR spectra of OVA, PEC, VD_3, OVA-PEC, OVA-VD_3 and OVA-PEC-VD_3 nanocomplexes.

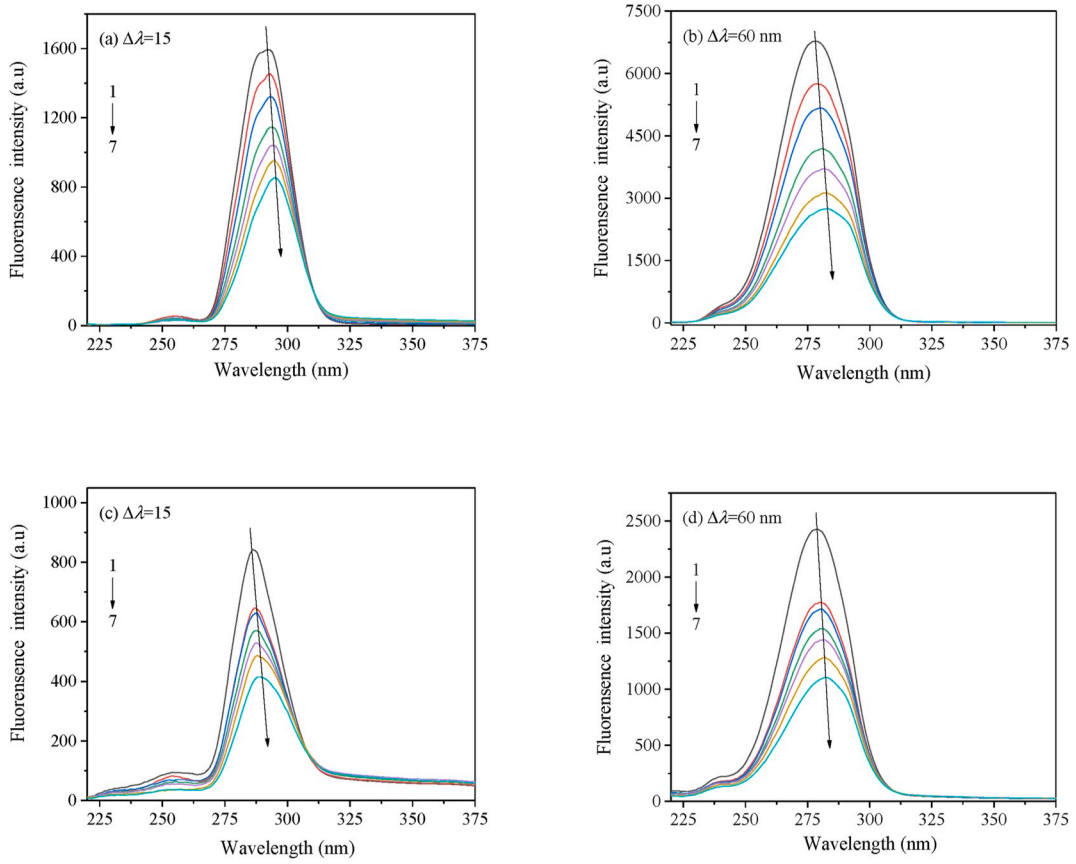

Fig. 8. Synchrotron fluorescence spectra. (a) and (b) are the effects of VD_3 on the synchronous fluorescence spectra of OVA, and (c) and (d) are the effects of VD_3 on the synchronous fluorescence spectra of OVA-PEC complexes.

Fernandez, & Luo, 2016; Hu, Wang, Zhou, Xue, & Luo, 2016). OVA is amphiphilic substance, and the characteristic peaks of hydrophilic hydroxyl groups in OVA appear at 3298 cm^{-1}, while the characteristic peaks of hydrophobic groups in OVA are ascribed to the $–CH_2$ stretching vibration at 2962 cm^{-1}. The peaks at 1649 cm^{-1} and 1535 cm^{-1} are the characteristic peaks of amide I band and the amide II band in OVA, respectively. The characteristic peaks of VD_3 mainly include sharp hydroxyl characteristic peak at 3308 cm^{-1} and $–CH_2$ characteristic peaks at 2933 cm^{-1} and 2867 cm^{-1}. In contrast to OVA, the –OH peaks of OVA-PEC, OVA-VD_3 and OVA-PEC-VD_3 nanocomplexes are significantly shifted, indicating the existence of hydrogen bonding interactions among OVA, PEC and VD_3. The characteristic peaks generated by asymmetric stretching of $–CH_2$ have a more significant blue shift in OVA-VD_3 complex than that of OVA-PEC complex, indicating that there is strong hydrophobic interaction between OVA and VD_3 (Zhou, Wang, & Hu, 2016). After the complex was formed, the amide I and amide II bands of OVA shifted to different degrees, which proved the existence of electrostatic interactions in the system. Thus the formation of OVA--PEC-VD_3 nanocomplexes is involved in the electrostatic interactions, hydrophobic interactions, and hydrogen bonding interactions among OVA, PEC, and VD_3.

4. Conclusion

In this work, the OVA-PEC-VD_3 nanocomplexes were fabricated to encapsulate and protect VD_3. The results showed that the encapsulation efficiency of VD_3 by OVA-PEC complexes is very high of 96.37%. The OVA-PEC-VD_3 nanocomplexes have good storage stability and achieves an ideal sustained-release effect in simulated gastrointestinal tract. A small amount of VD_3 is released in SGF, while a large amount of VD_3 is released in SIF validated by SEM and SDS-PAGE, which can help the body to digest and absorb VD_3. Modeling release kinetics in SGF and SIF demonstrated that the Higuchi model is reasonable and the release of VD_3 from OVA-PEC-VD_3 nanocomplexes is closer to Fick release. The formation mechanism of OVA-PEC-VD_3 nanocomplexes is ascribed to the electrostatic interactions, hydrogen bonding and hydrophobic interactions among OVA, PEC and VD_3. This work demonstrated that these nanocomplexes can be used in different nutritious food or beverage products to achieve a sustained release of vitamin, and increase the vitamin storage stability in the food matrix.

Declaration of competing interest

The authors declare no conflict of interest.

CRediT authorship contribution statement

Chuyue Xiang: Conceptualization, Data curation, Formal analysis, Writing - original draft. **Jian Gao:** Data curation, Formal analysis, Investigation, Methodology. **Haoxin Ye:** Data curation, Formal analysis. **Gerui Ren:** Investigation, Methodology. **Xiangjuan Ma:** Investigation, Formal analysis. **Hujun Xie:** Conceptualization, Funding acquisition, Project administration, Writing - original draft, Writing - review & editing. **Sheng Fang:** Conceptualization, Writing - original draft, Writing - review & editing. **Qunfang Lei:** Supervision, Writing - review & editing. **Wenjun Fang:** Supervision, Writing - review & editing.

Acknowledgements

This work was supported by the National Natural Science Foundation of China (Nos. 21203166 and 21473157). We are grateful to Professor Aiqian Ye from Massey University who provided fruitful discussions for this research.

Appendix A. Supplementary data

Supplementary data to this article can be found online at https://doi.org/10.1016/j.foodhyd.2020.105926.

References

Abbasi, A., Emam-Djomeh, Z., Mousavi, M. A. E., & Davoodi, D. (2014). Stability of vitamin D_3 encapsulated in nanoparticles of whey protein isolate. *Food Chemistry, 143*, 379–383.

Akyuz, L. (2020). An imine based cof as a smart carrier for targeted drug delivery: From synthesis to computational studies. *Microporous and Mesoporous Materials, 294*. https://doi.org/10.1016/j.micromeso.2019.109850.

Burey, P., Bhandari, B. R., Howes, T., & Gidley, M. J. (2008). Hydrocolloid gel particles: Formation, characterization, and application. *Critical Reviews in Food Science and Nutrition, 48*(5), 361–377.

Chang, C., Wang, T., Hu, Q., Zhou, M., Xue, J., & Luo, Y. (2017). Pectin coating improves physicochemical properties of caseinate/zein nanoparticles as oral delivery vehicles for curcumin. *Food Hydrocolloids, 70*, 143–151.

Chen, S., Li, Q., McClements, D. J., Han, Y. H., Dai, L., Mao, L. K., et al. (2020). Co-delivery of curcumin and piperine in zein-carrageenan core-shell nanoparticles: Formation, structure, stability and in vitro gastrointestinal digestion. *Food Hydrocolloids, 99*. https://doi.org/10.1016/j.foodhyd.2019.105334.

Chen, L. Y., Remondetto, G. E., & Subirade, M. (2006). Food protein-based materials as nutraceutical delivery systems. *Trends in Food Science & Technology, 17*(5), 272–283.

Cohen, Y., Levi, M., Lesmes, U., Margier, M., Reboul, E., & Livney, Y. D. (2017). Re-assembled casein micelles improve in vitro bioavailability of vitamin D in a Caco-2 cell model. *Food & Function, 8*(6), 2133–2141.

Delavari, B., Saboury, A. A., Atri, M. S., Ghasemi, A., Bigdeli, B., Khammari, A., et al. (2015). Alpha-lactalbumin: A new carrier for vitamin D_3 food enrichment. *Food Hydrocolloids, 45*, 124–131.

Diarrassouba, F., Remondetto, G., Li, L., Garrait, G., Beyssac, E., & Subirade, M. (2013). Effects of gastrointestinal pH conditions on the stability of the β-lactoglobulin/vitamin D_3 complex and on the solubility of vitamin D_3. *Food Research International, 52*(2), 515–521.

Fang, S., Zhao, X., Liu, Y., Liang, X., & Yang, Y. (2019). Fabricating multilayer emulsions by using OSA starch and chitosan suitable for spray drying: Application in the encapsulation of *β*-carotene. *Food Hydrocolloids, 93*, 102–110.

Feng, J., Xu, H. Q., Zhang, L. X., Wang, H., Liu, S. B., Liu, Y. J., et al. (2019). Development of nanocomplexes for curcumin vehiculization using ovalbumin and sodium alginate as building blocks: Improved stability, bioaccessibility, and antioxidant activity. *Journal of Agricultural and Food Chemistry, 67*(1), 379–390.

Higuchi, T. (1963). Mechanism of sustained-action medication - theoretical analysis of rate of release of solid drugs dispersed in solid matrices. *Journal of Pharmaceutical Sciences, 52*(12), 1145–1149.

Holick, M. F. (2007). Vitamin D deficiency. *New England Journal of Medicine, 357*(3), 266–281.

Huang, W. N., Wang, L. H., Wei, Y. Q., Cao, M. N., Xie, H. J., & Wu, D. (2020). Fabrication of lysozyme/κ-carrageenan complex nanoparticles as a novel carrier to enhance the stability and in vitro release of curcumin. *International Journal of Biological Macromolecules, 146*, 444–452.

Hu, Y. J., Liu, Y., Sun, T. Q., Bai, A. M., Lu, H. Q., & Pi, Z. B. (2006). Binding of anti-inflammatory drug cromolyn sodium to bovine serum albumin. *International Journal of Biological Macromolecules, 39*(4–5), 280–285.

Humblet-Hua, K. N. P., Scheltens, G., van der Linden, E., & Sagis, L. M. C. (2011). Encapsulation systems based on ovalbumin fibrils and high methoxyl pectin. *Food Hydrocolloids, 25*(4), 569–576.

Hu, S., Wang, T., Fernandez, M. L., & Luo, Y. (2016). Development of tannic acid cross-linked hollow zein nanoparticles as potential oral delivery vehicles for curcumin. *Food Hydrocolloids, 61*, 821–831.

Hu, Q., Wang, T., Zhou, M., Xue, J., & Luo, Y. (2016). In vitro antioxidant-activity evaluation of gallic-acid-grafted chitosan conjugate synthesized by free-radical-induced grafting method. *Journal of Agricultural and Food Chemistry, 64*(29), 5893–5900.

Jones, O. G., & McClements, D. J. (2010). Functional biopolymer particles: Design, fabrication, and applications. *Comprehensive Reviews in Food Science and Food Safety, 9*(4), 374–397.

Kaya, D., Kucukada, K., & Alemdar, N. (2019). Modeling the drug release from reduced graphene oxide-reinforced hyaluronic acid/gelatin/poly(ethylene oxide) polymeric films. *Carbohydrate Polymers, 215*, 189–197.

Levinson, Y., Ish-Shalom, S., Segal, E., & Livney, Y. D. (2016). Bioavailability, rheology and sensory evaluation of fat-free yogurt enriched with VD_3 encapsulated in re-assembled casein micelles. *Food & Function, 7*(3), 1477–1482.

Liang, H., Zhou, B., He, L., An, Y., Lin, L., Li, Y., et al. (2015). Fabrication of zein/quaternized chitosan nanoparticles for the encapsulation and protection of curcumin. *RSC Advances, 5*(18), 13891–13900.

Li, C. P., He, Z. K., Wang, X. Y., Yang, L., Yin, C. Y., Zhang, N., et al. (2014). Selenization of ovalbumin by dry-heating in the presence of selenite: Effect on protein structure and antioxidant activity. *Food Chemistry, 148*, 209–217.

Lii, C. Y., Chen, H. H., Lu, S., & Tomasik, P. (2003). Electrosynthesis of κ-carrageenan–ovalbumin complexes. *International Journal of Food Science and Technology, 38*, 787–793.

Lin, L. F., Xu, W., Liang, H. S., He, L., Liu, S. L., Li, Y., et al. (2015). Construction of ph-sensitive lysozyme/pectin nanogel for tumor methotrexate delivery. *Colloids and Surfaces B: Biointerfaces, 126*, 459–466.

Liu, X. Y., Wu, X., & Yang, J. H. (2010). Protein determination using methylene blue in a synchronous fluorescence technique. *Talanta, 81*(3), 760–765.

Li, J. H., Zhang, Y. F., Fan, Q., Teng, C. H., Xie, W. Y., Shi, Y., et al. (2018). Combination effects of NaOH and NaCl on the rheology and gel characteristics of hen egg white proteins. *Food Chemistry, 250*, 1–6.

Martos, G., Contreras, P., Molina, E., & Lope-Fandino, R. (2010). Egg white ovalbumin digestion mimicking physiological conditions. *Journal of Agricultural and Food Chemistry, 58*(9), 5640–5648.

Maste, M. C. L., Norde, W., & Visser, A. J. W. G. (1997). Adsorption-induced conformational changes in the serine proteinase savinase: A tryptophan fluorescence and circular dichroism study. *Journal of Colloid and Interface Science, 196*(2), 224–230.

Niu, F., Dong, Y., Shen, F., Wang, J., Liu, Y., Su, Y., et al. (2015). Phase separation behavior and structural analysis of ovalbumin–gum Arabic complex coacervation. *Food Hydrocolloids, 43*, 1–7.

Papadopoulou, A., Green, R. J., & Frazier, R. A. (2005). Interaction of flavonoids with bovine serum albumin: A fluorescence quenching study. *Journal of Agricultural and Food Chemistry, 53*(1), 158–163.

Qiu, J. H., Zheng, Q. X., Fang, L., Wang, Y. B., Min, M., Shen, C., et al. (2018). Preparation and characterization of casein-carrageenan conjugates and self-assembled microcapsules for encapsulation of red pigment from paprika. *Carbohydrate Polymers, 196*, 322–331.

Rostami, M., Yousefi, M., Khezerloua, A., Mohammadi, M. A., & Jafaric, S. M. (2019). Application of different biopolymers for nanoencapsulation of antioxidants via electrohydrodynamic processes. *Food Hydrocolloids, 97*, 105170.

Ru, Q. M., Wang, Y. W., Lee, J., Ding, Y. T., & Huang, Q. R. (2012). Turbidity and rheological properties of bovine serum albumin/pectin coacervates: Effect of salt concentration and initial protein/polysaccharide ratio. *Carbohydrate Polymers, 88*(3), 838–846.

Sarkar, A., Zhang, S. N., Murray, B., Russell, J. A., & Boxal, S. (2017). Modulating in vitro gastric digestion of emulsions using composite whey protein-cellulose nanocrystal interfaces. *Colloids and Surfaces B: Biointerfaces, 158*, 137–146.

Schmidt, I., Novales, B., Boué, F., & Axelos, M. A. V. (2010). Foaming properties of protein/pectin electrostatic complexes and foam structure at nanoscale. *Journal of Colloid and Interface Science, 345*(2), 316–324.

Schmitt, C., Sanchez, C., Desobry-Banon, S., & Hardy, J. (1998). Structure and technofunctional properties of protein-polysaccharide complexes: A review. *Critical Reviews in Food Science and Nutrition, 38*(8), 689–753.

Schoener, A. L., Zhang, R., Lv, S., Weiss, J., & McClements, D. J. (2019). Fabrication of plant-based vitamin D3-fortified nanoemulsions: Influence of carrier oil type on vitamin bioaccessibility. *Food & Function, 10*(4), 1826–1835.

Souza, C. J. F., & Garcia-Rojas, E. E. (2015). Effects of salt and protein concentrations on the association and dissociation of ovalbumin-pectin complexes. *Food Hydrocolloids, 47*, 124–129.

Ström, A., Schuster, E., & Goh, S. M. (2014). Rheological characterization of acid pectin samples in the absence and presence of monovalent ions. *Carbohydrate Polymers, 113*, 336–343.

Vis, E. H., Plinck, A. F., Alink, G. M., & van Boekel, M. A. J. S. (1998). Antimutagenicity of heat-denatured ovalbumin, before and after digestion, as compared to caseinate, BSA, and soy protein. *Journal of Agricultural and Food Chemistry, 46*(9), 3713–3718.

Xie, H. J., Xiang, C. Y., Li, Y., Wang, L. H., Zhang, Y. T., Song, Z. J., et al. (2019). Fabrication of ovalbumin/κ-carrageenan complex nanoparticles as a novel carrier for curcumin delivery. *Food Hydrocolloids, 89*, 111–121.

Yang, M. L., Wu, Y., Li, J. B., Zhou, H. B., & Wang, X. Y. (2013). Binding of curcumin with bovine serum albumin in the presence of iota-carrageenan and implications on the stability and antioxidant activity of curcumin. *Journal of Agricultural and Food Chemistry, 61*(29), 7150–7155.

Yu, X., Yang, Y., Lu, S., Yao, Q., Liu, H., Li, X., et al. (2011). The fluorescence spectroscopic study on the interaction between imidazo 2,1-b thiazole analogues and bovine serum albumin. *Spectrochimica Acta Part A-Molecular and Biomolecular Spectroscopy, 83*(1), 322–328.

Zhou, M., Wang, T., Hu, Q., & Luo, Y. (2016). Low density lipoprotein/pectin complex nanogels as potential oral delivery vehicles for curcumin. *Food Hydrocolloids, 57*, 20–29.